Vortices in Bose-Einstein condensates with $\mathcal{PT}$-symmetric gain and loss

Lukas Schwarz,[1] Holger Cartarius,[1] Ziad H. Musslimani,[1,2] Jörg Main,[1] and Günter Wunner[1]

[1]*Institut für Theoretische Physik 1, Universität Stuttgart, Pfaffenwaldring 57, 70550 Stuttgart, Germany*
[2]*Department of Mathematics, Florida State University, Tallahassee, Florida 32306-4510, USA*

We investigate vortex excitations in dilute Bose-Einstein condensates in the presence of complex $\mathcal{PT}$-symmetric potentials. These complex potentials are used to describe a balanced gain and loss of particles and allow an easier calculation of stationary states in open systems than in a full dynamical calculation including the whole environment. We examine the conditions under which stationary vortex states can exist and consider transitions from vortex to nonvortex states. In addition, we study the influences of $\mathcal{PT}$ symmetry on the dynamics of nonstationary vortex states placed at off-center positions.

I. INTRODUCTION

Quantized vortices [1–3] are coherent excitations in Bose-Einstein condensates, which can arise due to the superfluid property of such a condensate. These are stationary flows characterized by their quantized circulation

$$\Gamma = \oint \vec{v} \cdot d\vec{r} = \oint \frac{\hbar}{m} \boldsymbol{\nabla} S \cdot d\vec{r} = \frac{2\pi\hbar}{m} n, \qquad n \in \mathbb{N}, \quad (1)$$

where $\vec{v} = \vec{j}/\rho$ is the probability current velocity, $\vec{j}$ the probability current density, ρ the probability density, and S the phase of the wave function $\psi = \sqrt{\rho}\, e^{iS}$. Vortices in Bose-Einstein condensates have been studied theoretically [4–6] since the introduction of mean-field theory for Bose-Einstein condensates. Later on, several techniques to create vortices experimentally were proposed and also realized such as rotating traps [7–9], stirring condensates via laser beams [10,11], phase imprinting techniques [12,13], and temperature quenching via the Kibble-Zurek mechanism [14,15].

In this paper vortices are investigated in the presence of coherent balanced gain and loss of particles described via complex $\mathcal{PT}$-symmetric potentials. The $\mathcal{PT}$-symmetric formulation of quantum mechanics was introduced by Bender and Boettcher in 1998 [16], where they found that the requirement of a Hermitian Hamiltonian is not the most general condition to ensure real energy eigenvalues required for a physical theory. It can be shown [17] that a Hamiltonian which possesses an unbroken $\mathcal{PT}$ symmetry has purely real eigenvalues. Here, the unbroken $\mathcal{PT}$ symmetry is defined in such a way that $[H,\mathcal{PT}] = 0$ and in addition all eigenfunctions of the Hamiltonian are simultaneously eigenfunctions of the $\mathcal{PT}$ operator. Such a Hamiltonian is called pseudo-Hermitian [18–20] and allows for complex potentials if the real and imaginary parts are symmetric and antisymmetric functions of the position vector $\vec{r}$, respectively.

An imaginary part of a potential is generally interpreted as an additional gain-loss term. This can be understood if one calculates the continuity equation for the (non)linear Schrödinger equation with a complex potential. After a short calculation one obtains

$$\partial\rho + \boldsymbol{\nabla}\vec{j} = 2\rho\,\mathrm{Im}V. \qquad (2)$$

The imaginary part of the potential acts as an additional source or drain term in the range where it overlaps with

the wave function. A $\mathcal{PT}$-symmetric situation differs from a general complex potential in such a way that the gain and loss contributions are balanced. This allows for stationary states with real energies, and $\mathcal{PT}$ symmetry is used as an effective theory for an easier description of this dynamical process within the framework of stationary equations.

Since the discovery of Bender and Boettcher, $\mathcal{PT}$ symmetry has become important in many areas of physics. Most theoretical studies are in the fields of quantum mechanics [21–24] or quantum field theories [25,26]. Nonlinear $\mathcal{PT}$-symmetric quantum systems have been discussed for Bose-Einstein condensates described in a two-mode approximation [27,28], in position space [29–31], and in model potentials [32]. However, the concept of $\mathcal{PT}$ symmetry could also be studied in microwave cavities [33] and electronic devices [34].

In optics, the idea of $\mathcal{PT}$ symmetry can be applied as well to describe wave guides with complex refractive indices [35–38], and it is possible to observe this experimentally [39–41]. By contrast, an experimental confirmation of $\mathcal{PT}$ symmetry in a quantum mechanical system is still lacking. However, if $\mathcal{PT}$ symmetry is applied to the nonlinear Gross-Pitaevskii equation to describe a dilute Bose-Einstein condensate [29,42], the gain and loss can be interpreted as a coherent in- and outcoupling of particles, which may be possible to implement experimentally [30,43–45]. Therefore, Bose-Einstein condensates are good candidates for the first quantum mechanical system to observe $\mathcal{PT}$ symmetry.

In a number of works it has also been shown that even vortices are found in nonlinear $\mathcal{PT}$-symmetric systems [46–48]. However, most studies were done for optical setups, where coupled wave guides forming a discrete periodic structure were used [46,49–52]. It is the goal of this work to demonstrate that stable vortex excitations in Bose-Einstein condensates with $\mathcal{PT}$-symmetric gain and loss can exist. We will study the influence of the in- and outcoupling strength on stationary states as well as on the dynamics of nonstationary states. To do so we start with a vortex solution in a harmonic trap and then investigate how it behaves if this stable situation is disturbed by a current of particles. In contrast to systems with an azimuthal complex potential, where the degeneracy between opposite directions of rotation is lifted [53,54], this is not the case in our approach, where we are interested in a flow from one side of the trap to the other. This models a vortex being formed in a trap of a larger transport chain

similar to the proposal presented in [44,45] for the generation of a $\mathcal{PT}$-symmetric potential.

This paper is organized as follows. In Sec. II we introduce the model and explain the numerical techniques used. In Sec. III we show and discuss two qualitatively different spectra containing vortices arising due to different imaginary potentials. Additionally, the transition from vortex to non-vortex states at a critical gain-loss parameter value and the influence of the interaction strength are explained. In Sec. IV we investigate the stability of states using the Bogoliubov-de Gennes formalism and a time evolution. In Sec. V the dynamics of nonstationary vortex states in the presence of a $\mathcal{PT}$-symmetric potential is studied. Finally, in Sec. VI we summarize the obtained results.

II. MODEL

We consider a dilute Bose-Einstein condensate with contact interaction, which is described in the mean-field limit by the Gross-Pitaevskii equation. We assume that the condensate is confined in a harmonic oscillator trap,

$$V_T(\vec{r}) = \frac{m}{2} \left[\omega_0^2 (x^2 + y^2) + \omega_z^2 z^2 \right], \tag{3}$$

where $\omega_z \gg \omega_0$. Therefore, the condensate will be disk-shaped and the description can be effectively reduced to two dimensions [55–58]. In addition, an imaginary potential V_I is present, which describes the in- and outcoupling of particles. With the use of harmonic oscillator units,

$$\vec{r} \rightarrow \frac{\vec{r}}{r_0}, \qquad r_0 = \sqrt{\frac{\hbar}{m \omega_0}}, \tag{4}$$

$$\mu \rightarrow \frac{\mu}{\mu_0}, \qquad \mu_0 = \frac{\hbar^2}{2m r_0^2}, \tag{5}$$

the dimensionless effectively two-dimensional stationary Gross-Pitaevskii equation reads

$$[-\nabla^2 + V_T + i \Gamma V_I + g|\psi|^2] \psi = \mu \psi, \tag{6}$$

with

$$\psi = \psi(x,y), \qquad \iint |\psi(x,y)|^2 \, dx \, dy = 1, \tag{7}$$

and the effective two-dimensional chemical potential μ. The trap potential reads in these units

$$V_T = V_T(x,y) = x^2 + y^2, \tag{8}$$

and the interaction strength is $g = 8\pi N a / r_0$, where $a > 0$ is the effective two-dimensional repulsive s-wave scattering length. All quantities used in this article are given in these dimensionless units. The parameter Γ determines the strength of the gain and loss.

We investigate several different imaginary parts V_I. Specifically, we will use three different potentials labeled (a), (b), (c) to discuss the observed properties. They read

$$V_{I,a}(x,y) = x e^{-(x^2+y^2)}, \tag{9a}$$

$$V_{I,b}(x,y) = x^3 e^{-(x^2+y^2)}, \tag{9b}$$

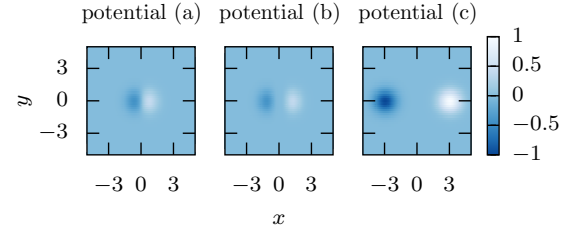$$V_{I,c}(x,y) = e^{-(x-d)^2 - y^2} - e^{-(x+d)^2 - y^2}, \tag{9c}$$

FIG. 1. The three example potentials from Eq. (9) used in this work. For potential (c) the parameter is $d = 3$.

and are shown in Fig. 1. These potentials represent an incoupling on the right and an outcoupling on the left side. Thus, we expect a current from right to left.

To solve the Gross-Pitaevskii equation numerically, this partial differential equation was discretized and expressed in a harmonic oscillator basis, in which the problem reduces to a high-dimensional nonlinear root search. This works quite well because the potential is mainly harmonic oscillator-like and we are considering not too large nonlinearities. Here, a two-dimensional-harmonic oscillator product basis up to the quantum numbers $n_{\max} = 11$ was used, which results in $N_{\text{states}} = 78$ basis states. For the calculation the quadratic field of view was set to $x,y \in [-5,5]$ and discretized with $N = 128$ points.

We are interested in low-lying excited states, therefore initial guesses for the root search are the harmonic oscillator ground state, the first excited state oriented in the x direction as well as its counterpart in the y direction. A superposition of the two first excited states, one as real and one as imaginary part to imprint a vortex phase, is used as an initial guess for a vortex state.

III. STATIONARY STATES AND SPECTRA

First the interaction strength is fixed to $g = 1$ and the parameter Γ is varied to study the influence of the gain-loss effect. This results in two qualitatively different spectra dependent on the chosen imaginary part. Numerical examples of the potentials (9a) and (9b) are shown in Fig. 2.

What is common for all investigated potentials is that there is a range of the gain-loss parameter Γ in which a vortex state exists. Actually, there are two vortex states which are degenerate since their only difference is their direction of circulation. However, at a critical value of Γ the vortex merges with the lowest excited state in a pitchfork bifurcation. Note that this is a standard pitchfork bifurcation. The two vortices with positive and negative circulation have identical stability properties. Since they are on top of each other when the chemical potential is plotted as in Fig. 2 they are only seen as one state. In the following we restrict our discussion to the state with positive circulation.

The state with which the vortex merges depends on the potential. If the in- and outcoupling peaks lie close to the origin, the excited state oriented parallel to the direction of the external current (excited x state) has lower chemical potential than the excited state oriented perpendicular to the external current (excited y state). For larger distances from the origin the order of the energy values changes. In addition, the distance has
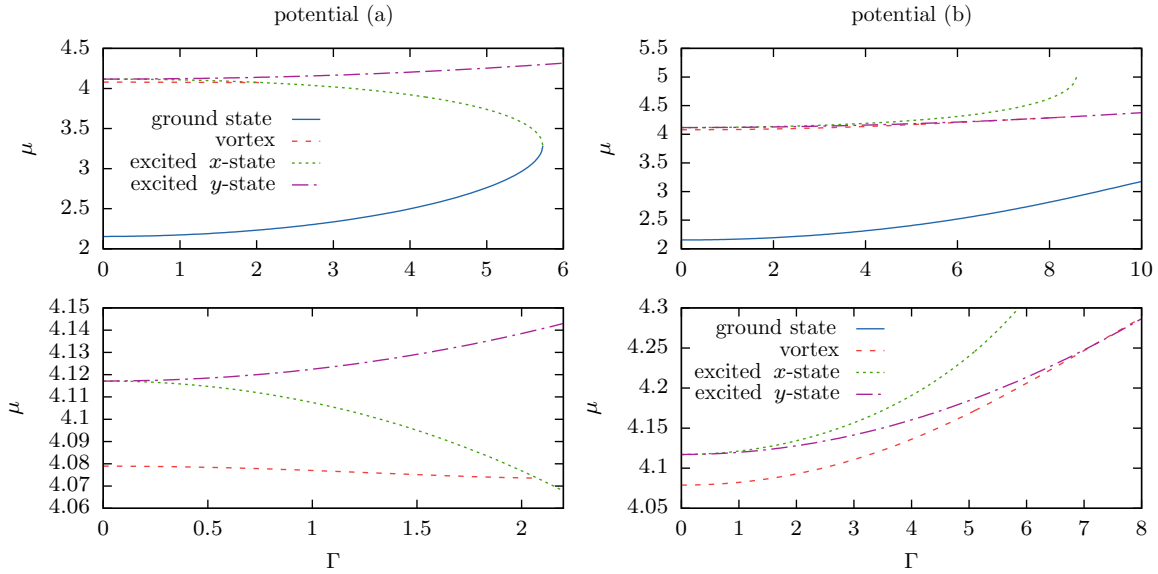
FIG. 2. Spectra as a function of the gain-loss strength Γ with the imaginary potentials (9a) (left) and (9b) (right) of the lowest states for $g = 1$. The lower figures are extracts of the upper figures in the range of the bifurcation between the vortex and the excited state. The two degenerate vortex states are shown as a single state.

an influence on a second tangent bifurcation of the excited state oriented in the x direction with the ground state. This bifurcation exists only for shorter distances of the gain-loss peaks from the origin; for larger values there is no such bifurcation.

A. Influence of gain-loss peak position d

Let us first discuss how the two qualitatively different spectra arise. For this analysis we use the potential (9c) with the variable distance d of the gain-loss peaks. We fix the gain-loss strength to $\Gamma = 2$ and vary the distance d. In Fig. 3 the chemical potential μ as well as the individual contributions of the average value of the kinetic and potential operator,

$$E_{\text{kin}} = \int |\nabla \psi|^2 \, d\vec{r}, \qquad E_{\text{pot}} = \int V |\psi|^2 \, d\vec{r}, \qquad (10)$$

are shown as functions of d, and in Fig. 4 the excited states and the potential are shown for selected values of d.

For this example the imaginary part vanishes for $d = 0$, as the in- and outcoupling peaks cancel each other. Therefore, the x and y states become degenerate. For increasing d the in- and outcoupling peaks lie close to the origin at first. This causes a shift of the probability density of the x state to the origin, which results in a decrease in the potential energy. As the gain-loss peaks are oriented in the x direction, the y state does not experience such a shift and the potential energy does not drop.

At some value of d, the gain-loss peaks exceed the point at which the positions of the x-state peaks without complex potential are located. Behind this point the x-state probability density is shifted outward again, which leads to an increase of the potential energy. The y state is again not substantially affected.

Eventually at a value of $d \approx 1.37$, the increase in the potential energy of the x state leads to a higher chemical

potential μ than that of the y state. For even higher d the peaks move out of the probability density range of the wave functions and the influence, i.e., the in- and outcoupling, vanishes. The chemical potentials of the two states approach each other again.

This explains also why the second bifurcation of the ground and an excited state only occurs for the excited x state. The ground state resembles the excited y state in the x direction and behaves similar to the excited y state, i.e., it is also less affected by the gain-loss. Due to this similar behavior, the distance between their chemical potentials cannot change as
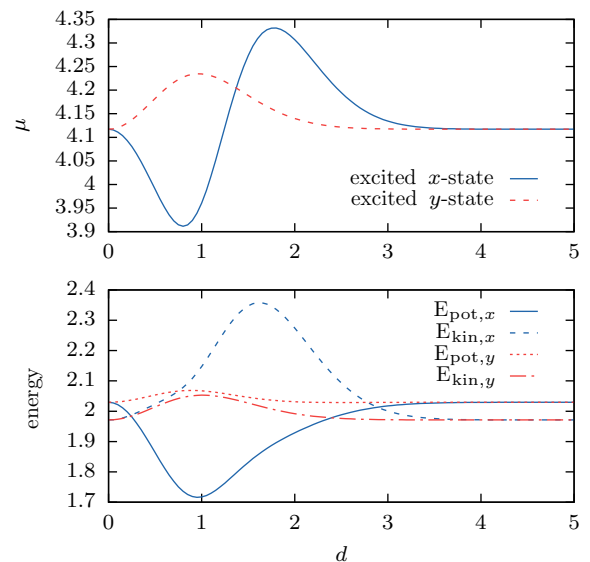

FIG. 3. Chemical potential (top) and the individual contributions E_{kin} and E_{pot} (bottom) of the excited states as a function of the gain-loss peaks position d from the imaginary potential (9c). The parameters are $g = 1$ and $\Gamma = 2$.
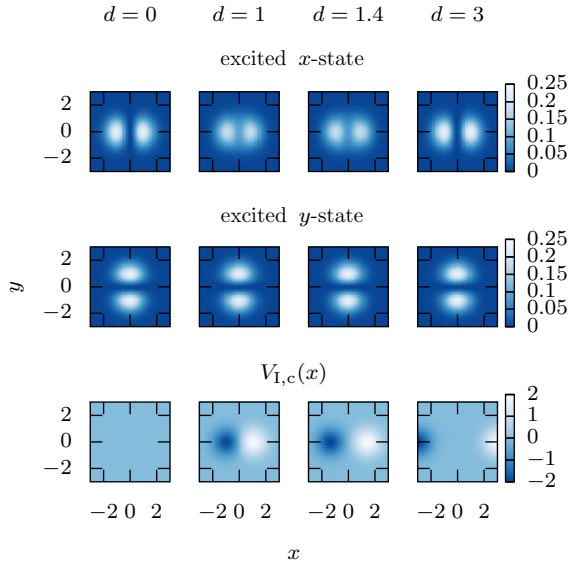
FIG. 4. Modulus squared of the wave functions of the excited states in potential (9c) (upper two rows) and the corresponding potentials (lower row) for different values of the gain-loss peaks position d. The parameters are $g = 1$ and $\Gamma = 2$.

much as between the excited x state and the ground state; therefore, these states do not coalesce.

B. Transition of vortex to nonvortex state

Now we discuss the transition of vortex to nonvortex states. The bifurcation point, at which the vortex changes to an excited state without vorticity, marks a so-called exceptional point [59–64]. At this point not only the energies but also the states themselves coalesce. This is a feature which cannot occur in Hermitian systems but can result in non-Hermitian or nonlinear Hamiltonians.

To explain this transition it is useful to consider the wave function and phase as well as the probability current density calculated with

$$\vec{j} = i(\psi \nabla \psi^* - \psi^* \nabla \psi). \tag{11}$$

These quantities are shown in Fig. 5 for the potentials (9a) and (9b) for different values of the gain-loss parameter Γ. For $\Gamma = 0$, i.e., no gain-loss, the vortex solutions are totally symmetric and positioned at the origin. Only the circular vortex current is present.

For increasing Γ the behavior slightly differs depending on the imaginary potential. In the case of the bifurcation with the x-excited state [Fig. 5 (left)], the vortex center shifts toward the bottom. For the (not shown) vortex with opposite circulation the center shifts toward the top. Due to the additional current from right to left, the shape of the vortex adapts itself in such a way that the probability density on the top is higher than that on the bottom by shifting the vortex center. Therefore, the natural vortex current is enhanced from right to left at the top, while the current is suppressed from left to right at the bottom. The basic shape of the wave function becomes more and more asymmetric in the y direction. The whole solution is cut into two parts. Finally, the vortex center is expelled in the region at the wave function's border, at which the probability density vanishes. At that point the vortex decays and changes into the first excited state with the two peaks on the left and right of the origin. The vortex current from left to right at the bottom comes to a halt because the external current is stronger than the vortex current.

This becomes also visible in Fig. 6, in which the integrated projection

$$J_\varphi = \int \vec{j} \cdot \vec{e}_\varphi \, d\vec{r} \tag{12}$$

of the current density on the azimuthal direction is shown as a function of Γ. While this vanishes for the excited x state it has a nonvanishing value for the vortex from Fig. 5(a). For the vortex the value of J_φ remains almost constant in a large range of Γ. Close to the bifurcation it rapidly starts to decrease and drops to zero at the bifurcation point confirming the transition from a vortex to a nonvortex state.

The transition from the vortex to the excited state in the y direction [Fig. 5 (right)] occurs in a different way. Here the vortex center performs only a slight movement in the y direction but then returns back to the center. An ejection in the x direction, which would be the nodal line for the excited y state, was not possible since a movement of the vortex center in this direction would break the $\mathcal{PT}$ symmetry of the wave
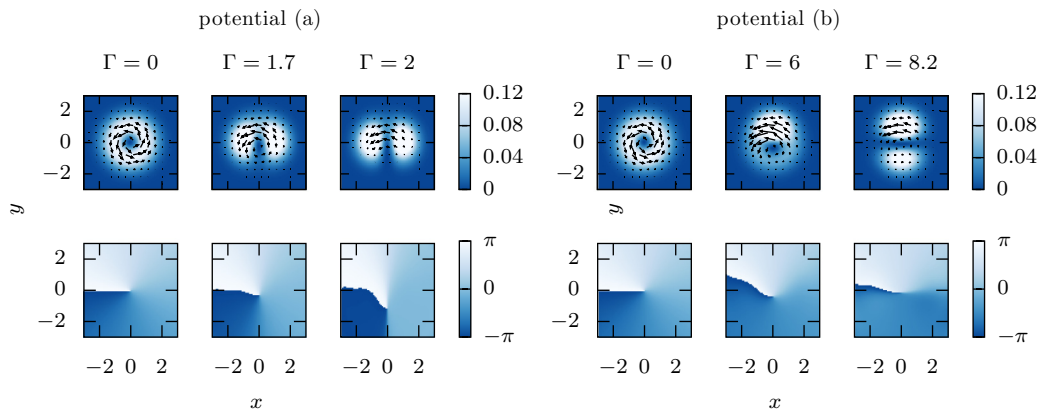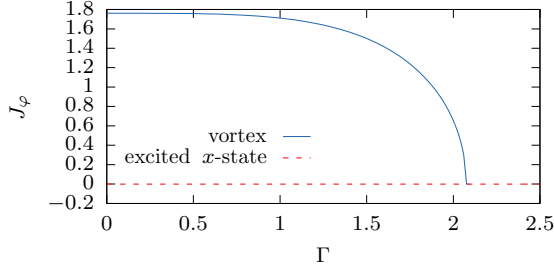

FIG. 5. Modulus squared of the wave functions with arrows representing the current density (top) and phase (bottom) for the imaginary potential (9a) (left) and (9b) (right) for different values of the gain-loss strength Γ. The nonlinearity is $g = 1$.

FIG. 6. Integrated projection J_φ of the current density on the azimuthal direction for the vortex from Fig. 5(a). It starts with a nonvanishing value for the vortex clearly distinguishing it from the excited x state. Close to the bifurcation it rapidly decreases to zero.

function. What happens is that the probability density nearly drops to zero in the lower half of the vortex, in which the current flows in opposite direction to the external current. This brings the circular vortex current to a halt and the vortex dies at its location. Thus, the vortex does not vanish as a result of the center ejection but simply by stopping the current in one direction while the center stays on the nodal line of the excited y state.

C. Influence of the interaction strength g

After having fixed $g = 1$ in the previous examples, now the influence of higher interaction strengths will be discussed. What can we expect? As we are considering repulsive interaction, a higher strength will spread the wave function more to the outside. We have shown that the type of spectrum we obtain depends on the position d of the in- and outcoupling peaks relative to the natural wave-function position without gain and loss. Therefore, at a small fixed distance d an increase of g should not change the spectra qualitatively since the in- and outcoupling peaks are located inside the wave function's maxima anyway. In the case of the second spectra from Fig. 2 (right side) for large d, a qualitative transition to the type of the first spectra may occur because the probability density of the wave function can be shifted beyond the in- and outcoupling peaks. However, this is something which happens not in every case and depends on the actual form of the imaginary part.

For the example potentials (9a) and (9b) the spectra for different values of g can be found in Fig. 7. In both cases the separation between vortex and excited state increases for increasing nonlinearity. This results from the fact that due to the two strongly located peaks of the excited states in comparison to the more blurred vortex, the interaction energy of the excited states increases more for higher interaction strength. Therefore, the vortex states become energetically more favorable for increasing g.

The spectra for potential (9a) stay qualitatively the same, while for potential (9b) a transition of the spectra type can be observed. However, as already mentioned, this is not what happens in general. Calculations with different potentials do not always show such a transition. To be precise, in these cases the excited x state may be located below the excited y state in some regions, but eventually the positions switch again.

IV. STABILITY ANALYSIS

In reality the system cannot be perfectly isolated and there will always be small fluctuations. They may be observed experimentally only if the states survive within such an environment and live for a sufficiently long time. Therefore, it is important to check the stability of the states.

First the linear stability is checked using the Bogoliubov-de Gennes formalism. Within this formalism, a small time-dependent fluctuation $\Delta(\vec{r},t)$ is added to a stationary state $\psi_0(\vec{r})$

$$\psi(\vec{r},t) = [\psi_0(\vec{r}) + \Delta(\vec{r},t)]e^{-i\mu t}, \qquad (13)$$

where one uses the ansatz

$$\Delta = \epsilon(u(\vec{r})e^{-i\omega t} + v^*(\vec{r})e^{i\omega^* t}) \qquad (14)$$

with a positive value $\epsilon \ll 1$. Inserting this ansatz into the time-dependent Gross-Pitaevskii equation and neglecting terms in the order of $O(\epsilon^2)$ one obtains the linear Bogoliubov-de Gennes equations, which can be written in matrix form as

$$\begin{pmatrix} A & B \\ -B^* & -A^* \end{pmatrix} \begin{pmatrix} u \\ v \end{pmatrix} = \omega \begin{pmatrix} u \\ v \end{pmatrix} \qquad (15)$$

with

$$A = -\nabla^2 + V_{\mathrm{T}} + i\Gamma V_{\mathrm{I}} + 2g|\psi_0|^2 - \mu, \qquad (16)$$

$$B = g\psi_0^2. \qquad (17)$$

This linear eigenvalue problem can again be expressed and diagonalized in a harmonic oscillator basis. If there are solutions with complex frequencies ω, the fluctuations will exponentially increase, which is a clear sign of an unstable state. Due to the $\mathcal{PT}$ symmetry, if ω is a solution, then $-\omega$, ω^*, and $-\omega^*$ are also solutions; therefore, it is sufficient to consider only ω with positive imaginary part.

In Fig. 8 the imaginary eigenvalues are shown for the two different spectra for potentials (9a) and (9b). In the first case, the ground and the vortex state are always stable. The excited x state is unstable in the range where it coexists with the vortex but becomes stable after the bifurcation point. In the second case the vortex is not stable over the whole range in which it exists. Only for smaller values of Γ is it stable; at a value of $\Gamma \approx 2.7$ there is an unstable region until the end of the vortex existence.

To consider also nonlinear fluctuations and confirm the Bogoliubov-de Gennes analysis, a time evolution is performed. We take the exact eigenstates, add random noise, and let it evolve in time. If the state is stable, it will only perform small fluctuations or slightly oscillate but keep its basic shape over time, whereas an unstable state will completely deform or decay.

The time evolution is performed using the split-operator method, where the time evolution operator $U = \exp(-iHt)$ is split symmetrically for a small time step dt as

$$U(dt) \approx e^{-i\frac{-\nabla^2}{2}dt}e^{-i\tilde{V}dt}e^{-i\frac{-\nabla^2}{2}dt} + O(dt^3), \qquad (18)$$

with

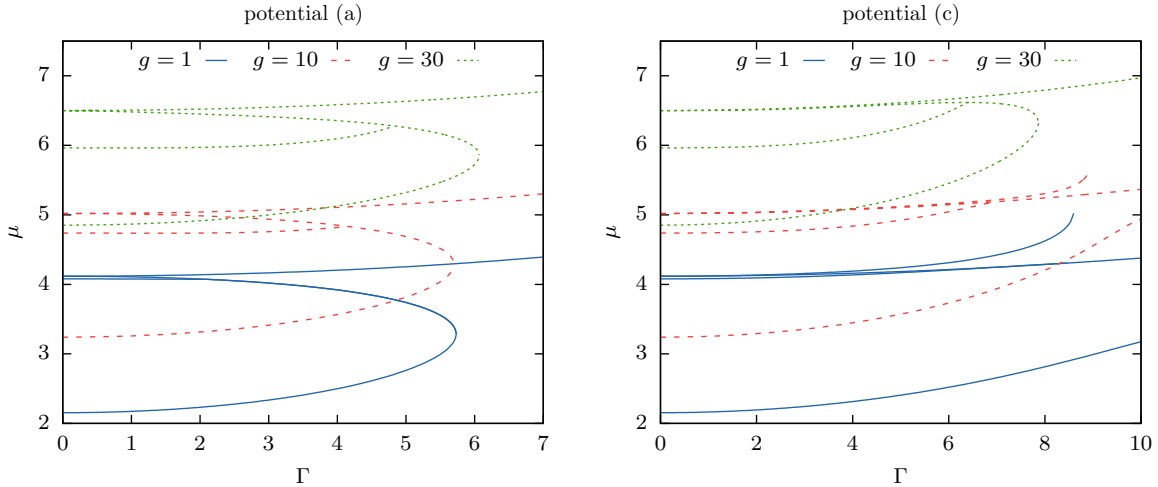$$\tilde{V} = V_{\mathrm{T}} + i\Gamma V_{\mathrm{I}} + g|\psi_0|^2. \qquad (19)$$

FIG. 7. Spectra dependent on the gain-loss strength Γ of the lowest states for potentials (9a) (left) and (9b) (right) for different values of the nonlinearity g. For potential (9a), the spectrum stays qualitatively the same independent of g. The spectrum for potential (9c) changes qualitatively to the spectrum for potential (9a) for increasing g.

This expression is evaluated with forward and backward Fourier transforms

$$\psi(dt) = U(dt)\psi_0$$
$$\approx \mathcal{F}^{-1}[e^{-i\frac{|\vec{k}|^2}{2}dt}\mathcal{F}[e^{-i\tilde{V}dt}\mathcal{F}^{-1}[e^{-i\frac{|\vec{k}|^2}{2}dt}\mathcal{F}[\psi_0]]]]. \quad (20)$$

As we work with a finite grid, reflections at the border or wraparounds in the Fourier space can occur. These artifacts can be reduced by increasing the discretization range or introducing absorbing borders [65]. However, in this case it is not necessary to remove all the artifacts, since they can be considered as additional distortions. This confirms the stability of states even more if they survive under this condition. In our case, only for potential (9b) for values of $\Gamma \gtrsim 2$ does the discretization range have to be doubled to $x, y \in [-10, 10]$ and $N = 256$ grid points in each direction to allow the required calculations.

In Fig. 9 the time evolution of the distorted vortex states is depicted for different values of the gain-loss parameter Γ. In each case random data on the order of 10^{-2} are added to the initial state. The time evolution is performed over 1000 time steps with a step size of $dt = 10^{-3}$. The distorted initial state and the final state after the time evolution are shown. This time evolution confirms the result from the Bogoliubov-de Gennes analysis. For potential (9a) the vortex state is stable independently of Γ, whereas for potential (9b) the state is stable only for smaller values of Γ and finally becomes unstable.
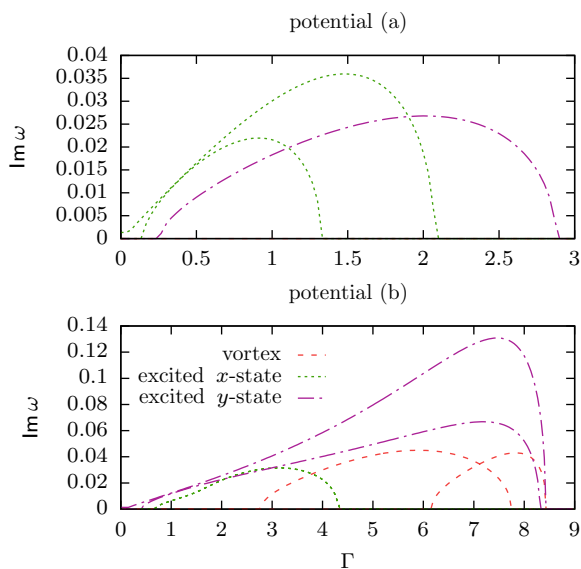

FIG. 8. Positive imaginary parts of the Bogoliubov-de Gennes eigenvalues ω for potentials (9a) (top) and (9b) (bottom). The nonlinearity is $g = 1$. The ground state is always stable and has no imaginary contribution.
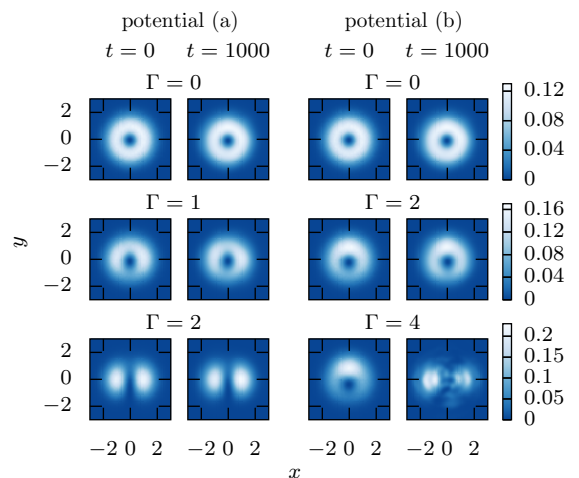

FIG. 9. Time evolution for 1000 time steps of the stationary vortex state of potentials (9a) (left) and (9b) (right) for $g = 1$ and different values of Γ. The initial state is distorted with random noise on the order of 10^{-2} and propagated with the split-operator method with a step size of $dt = 10^{-3}$.

V. DYNAMICS

Lastly, we study the dynamics of nonstationary vortex states in a $\mathcal{PT}$-symmetric potential. We ask how a vortex reacts and evolves in time in the presence of a balanced net current through the condensate.

Vortex movement has already been discussed in the literature [2,66–68] and there are several facts known. The motion of a Bose-Einstein condensate with its center of mass positioned out of the trap center can be described like that of a classical single particle in an effective potential [66,69,70]. The movement of the particle corresponds to the center of mass movement of the condensate. A movement of the vortex relative to its background causes a Magnus force on the vortex perpendicular to its velocity [71], which results in a precession around the trap center. The Magnus force has a hydrodynamic cause created by a pressure gradient resulting from a suppression and an enhancement of the vortex current on the opposite sites.

For our study we use potential (9c) with $d = 1$. First we set the gain-loss parameter $\Gamma = 0$ and place a vortex initially at an off-center position via

$$\psi = [(x - x_0) + i(y - y_0)]e^{-\frac{1}{2}(x^2 + y^2)} \tag{21}$$

and let it propagate in time. The position of the vortex center is determined via a parabolic fit at the minimum. The resulting trajectory can be found in the first plot of Fig. 10. The expected circular motion around the trap center can clearly be observed.

Now we turn on the external current via our $\mathcal{PT}$-symmetric complex potential, i.e., $\Gamma \neq 0$. The resulting trajectory for two different values of Γ can be seen in the middle plots of Fig. 10 with the same initial vortex as in the previous case. Despite the additional current, one can see that a stable movement is still possible. The circular trajectory is slightly distorted which results from the fact that our initial symmetric vortex is a bad approximation of the asymmetric stationary vortex. This results in deformation of the background cloud and an additional movement of the vortex.

There is a second feature, which is not so obvious at first glance. The precession of the vortex is no longer symmetric regarding the origin, but with respect to a point slightly below. The whole trajectory is shifted. This can be understood by remembering the stationary solutions calculated in Sec. IV. There we found that the eigenstates are also no longer symmetric in the y direction but the vortex center is shifted. Because of this, the equilibrium point is no longer the origin but

a point below it. Consequently, the precession occurs around this new equilibrium point.

The $\mathcal{PT}$-symmetric gain-loss is crucial for a stable movement. If we explicitly break the $\mathcal{PT}$ symmetry, e.g., by increasing the strength of the incoupling slightly,

$$V_I(x,y) = 1.2e^{-(x-d)^2 - y^2} - e^{-(x-d)^2 - y^2}, \tag{22}$$

two things can be observed. On the one hand the background grows because more particles are inserted than removed. On the other hand the trajectory becomes unstable, which can be seen in the last plot in Fig. 10.

The vortex spirals out until it hits the cloud border and vanishes. A $\mathcal{PT}$-broken gain and loss has a destabilizing effect on the movement and the trajectory becomes unstable.

VI. CONCLUSION

In this paper we demonstrated that stationary vortex states in Bose-Einstein condensates with balanced gain and loss of particles can exist. Independent of the actual form of the imaginary potential, we found always a range of the in- and outcoupling strength Γ which allows for the existence of stable vortices. If this parameter exceeds a critical value, i.e., the point at which the additionally introduced external current is stronger than the internal vortex current, the vortex decays. In the presence of the external current the stationary vortex adapts itself in such a way that it shifts its vortex center and changes the background shape such that a net current exists. If the vortex decays it changes into the energetically closest excited state, which manifests itself in a bifurcation and an exceptional point in the spectra.

A time evolution of nonstationary vortex states in the presence of $\mathcal{PT}$-symmetric potentials showed that the external current shifts the precession center of the vortex movement. This center corresponds to the position of the stationary vortex center and is the new equilibrium point of the dynamics. A balanced gain and loss is crucial for a stable movement, because unbalanced gain and loss leads to an unstable dynamics shown through an outward spiraling and decay of the vortex.
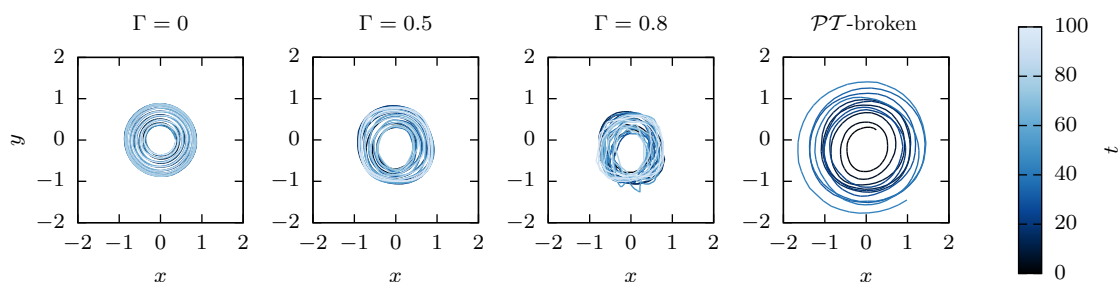
FIG. 10. Vortex dynamics of the nonstationary state (21) with $x_0 = y_0 = 0.2$. The first three plots are results for potential (9c) with $d = 1$ and $\Gamma = 0$, $\Gamma = 0.5$, and $\Gamma = 0.8$. The fourth plot is the result for the $\mathcal{PT}$-broken potential (22) with $\Gamma = 0.5$. In each plot the vortex center trajectory is shown as a function of time. The time evolution was performed with the split-operator method with a step size of $t = 10^{-3}$.

[1] F. Dalfovo, S. Giorgini, L. P. Pitaevskii, and S. Stringari, Rev. Mod. Phys. **71**, 463 (1999).

[2] A. L. Fetter and A. A. Svidzinsky, J. Phys. Condens. Matter **13**, R135 (2001).

[3] P. G. Kevrekidis, R. Carretero-Gonzáles, D. J. Frantzeskakis, and I. G. Kevrekidis, Mod. Phys. Lett. B **18**, 1481 (2004).

[4] L. P. Pitaevskii, Sov. Phys. JETP **13**, 451 (1961).

[5] E. P. Gross, Il Nuovo Cimento **20**, 454 (1961).

[6] E. P. Gross, J. Math. Phys. **4**, 195 (1963).

[7] A. L. Fetter, Phys. Rev. **138**, A429 (1965).

[8] Y. Castin and R. Dum, Eur. Phys. J. D **7**, 399 (1999).

[9] A. L. Fetter, Rev. Mod. Phys. **81**, 647 (2009).

[10] M. R. Matthews, B. P. Anderson, P. C. Haljan, D. S. Hall, C. E. Wieman, and E. A. Cornell, Phys. Rev. Lett. **83**, 2498 (1999).

[11] B. M. Caradoc-Davies, R. J. Ballagh, and K. Burnett, Phys. Rev. Lett. **83**, 895 (1999).

[12] L. Dobrek, M. Gajda, M. Lewenstein, K. Sengstock, G. Birkl, and W. Ertmer, Phys. Rev. A **60**, R3381(R) (1999).

[13] A. E. Leanhardt, A. Görlitz, A. P. Chikkatur, D. Kielpinski, Y. Shin, D. E. Pritchard, and W. Ketterle, Phys. Rev. Lett. **89**, 190403 (2002).

[14] C. N. Weiler, T. W. Neely, D. R. Scherer, A. S. Bradley, M. J. Davis, and B. P. Anderson, Nature **455**, 948 (2008).

[15] M. Tylutki, S. Donadello, S. Serafini, L. P. Pitaevskii, F. Dalfovo, G. Lamporesi, and G. Ferrari, Eur. Phys. J. Spec. Top. **224**, 577 (2015).

[16] C. M. Bender and S. Boettcher, Phys. Rev. Lett. **80**, 5243 (1998).

[17] C. M. Bender, Contemp. Phys. **46**, 277 (2005).

[18] A. Mostafazadeh, J. Math. Phys. **43**, 205 (2002).

[19] A. Mostafazadeh, J. Math. Phys. **43**, 2814 (2002).

[20] A. Mostafazadeh, J. Math. Phys. **43**, 3944 (2002).

[21] C. M. Bender, S. Boettcher, and P. N. Meisinger, J. Math. Phys. **40**, 2201 (1999).

[22] M. Znojil, Phys. Lett. A **264**, 108 (1999).

[23] H. Mehri-Dehnavi, A. Mostafazadeh, and A. Batal, J. Phys. A **43**, 145301 (2010).

[24] H. F. Jones and E. S. Moreira Jr, J. Phys. A **43**, 055307 (2010).

[25] C. M. Bender, V. Branchina, and E. Messina, Phys. Rev. D **85**, 085001 (2012).

[26] P. D. Mannheim, Fortschr. Phys. **61**, 140 (2013).

[27] E. M. Graefe, U. Günther, H. J. Korsch, and A. E. Niederle, J. Phys. A **41**, 255206 (2008).

[28] E. M. Graefe, J. Phys. A **45**, 444015 (2012).

[29] D. Dast, D. Haag, H. Cartarius, G. Wunner, R. Eichler, and J. Main, Fortschr. Phys. **61**, 124 (2013).

[30] R. Gutöhrlein, J. Schnabel, I. Iskandarov, H. Cartarius, J. Main, and G. Wunner, J. Phys. A **48**, 335302 (2015).

[31] N. Abt, H. Cartarius, and G. Wunner, Int. J. Theor. Phys. **54**, 4054 (2015).

[32] Z. H. Musslimani, K. G. Makris, R. El-Ganainy, and D. N. Christodoulides, J. Phys. A **41**, 244019 (2008).

[33] S. Bittner, B. Dietz, U. Günther, H. L. Harney, M. Miski-Oglu, A. Richter, and F. Schäfer, Phys. Rev. Lett. **108**, 024101 (2012).

[34] J. Schindler, A. Li, M. C. Zheng, F. M. Ellis, and T. Kottos, Phys. Rev. A **84**, 040101 (2011).

[35] S. Klaiman, U. Günther, and N. Moiseyev, Phys. Rev. Lett. **101**, 080402 (2008).

[36] K. G. Makris, R. El-Ganainy, D. N. Christodoulides, and Z. H. Musslimani, Phys. Rev. Lett. **100**, 103904 (2008).

[37] Z. H. Musslimani, K. G. Makris, R. El-Ganainy, and D. N. Christodoulides, Phys. Rev. Lett. **100**, 030402 (2008).

[38] R. El-Ganainy, K. G. Makris, D. N. Christodoulides, and Z. H. Musslimani, Opt. Lett. **32**, 2632 (2007).

[39] A. Guo, G. J. Salamo, D. Duchesne, R. Morandotti, M. Volatier-Ravat, V. Aimez, G. A. Siviloglou, and D. N. Christodoulides, Phys. Rev. Lett. **103**, 093902 (2009).

[40] C. E. Rüter, K. G. Makris, R. El-Ganainy, D. N. Christodoulides, M. Segev, and D. Kip, Nat. Phys. **6**, 192 (2010).

[41] B. Peng, S. K. Ozdemir, F. Lei, F. Monifi, M. Gianfreda, G. L. Long, S. Fan, F. Nori, C. M. Bender, and L. Yang, Nat. Phys. **10**, 394 (2014).

[42] H. Cartarius and G. Wunner, Phys. Rev. A **86**, 013612 (2012).

[43] F. Single, H. Cartarius, G. Wunner, and J. Main, Phys. Rev. A **90**, 042123 (2014).

[44] M. Kreibich, J. Main, H. Cartarius, and G. Wunner, Phys. Rev. A **90**, 033630 (2014).

[45] M. Kreibich, J. Main, H. Cartarius, and G. Wunner, Phys. Rev. A **93**, 023624 (2016).

[46] V. V. Konotop, J. Yang, and D. A. Zezyulin, Rev. Mod. Phys. **88**, 035002 (2016).

[47] V. Achilleos, P. G. Kevrekidis, D. J. Frantzeskakis, and R. Carretero-González, Phys. Rev. A **86**, 013808 (2012).

[48] V. Achilleos, P. G. Kevrekidis, D. J. Frantzeskakis, and R. Carretero-González, in *Localized Excitations in Nonlinear Complex Systems: Current State of the Art and Future Perspectives*, edited by R. Carretero-González, J. Cuevas-Maraver, D. Frantzeskakis, N. Karachalios, P. Kevrekidis, and F. Palmero-Acebedo (Springer International, New York, 2014) pp. 3–42.

[49] A. A. Sukhorukov, S. V. Dmitriev, S. V. Suchkov, and Y. S. Kivshar, Opt. Lett. **37**, 2148 (2012).

[50] D. Leykam, V. V. Konotop, and A. S. Desyatnikov, Opt. Lett. **38**, 371 (2013).

[51] Z. Chen, J. Liu, S. Fu, Y. Li, and B. A. Malomed, Opt. Express **22**, 29679 (2014).

[52] Y. V. Kartashov, V. V. Konotop, V. A. Vysloukh, and L. Torner, Opt. Lett. **35**, 3177 (2010).

[53] Y. V. Kartashov, V. V. Konotop, and L. Torner, Phys. Rev. Lett. **115**, 193902 (2015).

[54] C. Huang and L. Dong, Opt. Lett. **41**, 5194 (2016).

[55] W. Bao, D. Jaksch, and P. A. Markowich, J. Comput. Phys. **187**, 318 (2003).

[56] N. B. Abdallah, F. Méhats, C. Schmeiser, and R. M. Weishäupl, SIAM J. Math. Anal. **37**, 189 (2005).

[57] W. Bao, Y. Ge, D. Jaksch, P. A. Markowich, and R. M. Weishäupl, Comput. Phys. Commun. **177**, 832 (2007).

[58] W. Bao, L. L. Treust, and F. Méhats, Nonlinearity **28**, 755 (2015).

[59] T. Kato, *Perturbation Theory for Linear Operators*, 2nd ed. (Springer-Verlag, Berlin, 1976).

[60] W. D. Heiss, J. Phys. A **45**, 444016 (2012).

[61] L. Schwarz, H. Cartarius, G. Wunner, W. D. Heiss, and J. Main, Eur. Phys. J. D **69**, 196 (2015).

[62] H. Menke, M. Klett, H. Cartarius, J. Main, and G. Wunner, Phys. Rev. A **93**, 013401 (2016).

[63] J. Doppler, A. A. Mailybaev, J. Böhm, U. Kuhl, A. Girschik, F. Libisch, T. J. Milburn, P. Rabl, N. Moiseyev, and S. Rotter, Nature **537**, 76 (2016).

[64] H. Xu, D. Mason, L. Jiang, and J. G. E. Harris, Nature **537**, 80 (2016).

[65] R. Kosloff and D. Kosloff, J. Comput. Phys. **63**, 363 (1986).

[66] P. G. Kevrekidis, R. Carretero-González, G. Theocharis, D. J. Frantzeskakis, and B. A. Malomed, J. Phys. B **36**, 3467 (2003).

[67] Y. S. Kivshar, J. Christou, V. Tikhonenko, B. Luther-Davies, and L. M. Pismen, Opt. Commun. **152**, 198 (1998).

[68] E. Lundh and P. Ao, Phys. Rev. A **61**, 063612 (2000).

[69] R. Carretero-González and K. Promislow, Phys. Rev. A **66**, 033610 (2002).

[70] D. J. Frantzeskakis, G. Theocharis, F. K. Diakonos, P. Schmelcher, and Y. S. Kivshar, Phys. Rev. A **66**, 053608 (2002).

[71] B. P. Anderson, P. C. Haljan, C. E. Wieman, and E. A. Cornell, Phys. Rev. Lett. **85**, 2857 (2000).